ACADEMIC PRESS

Available online at www.sciencedirect.com
SCIENCE DIRECT®

Journal of Catalysis 217 (2003) 406–416

JOURNAL OF CATALYSIS

www.elsevier.com/locate/jcat

On the shape selective acylation of 2-methoxynaphthalene over polymorph C of Beta (ITQ-17)

P. Botella, A. Corma,* M.T. Navarro, F. Rey, and G. Sastre

Instituto de Tecnología Química, UPV-CSIC, Universidad Politécnica de Valencia, Avda. de los Naranjos s/n, 46022 Valencia, Spain

Received 11 November 2002; revised 23 January 2003; accepted 23 January 2003

Abstract

2-Methoxynaphthalene (2-MN) has been acylated with acetic anhydride on polymorph C of Beta (ITQ-17), and 2-acetylmethoxynaphthalene (2-AMN) and 1-acetylmethoxynaphthalene (1-AMN) have been obtained. The diffusivity of the two isomer products, as determined by molecular dynamics, shows that the ratio of the diffusion coefficients for 2-AMN/1-AMN is one order of magnitude larger for polymorph C than for polymorphs A and B (Beta zeolite). This corresponds very well with experimental acylation results that show a higher selectivity for 2-AMN on polymorph C when reaction is carried out in batch as well as in a fixed-bed continuous reactor.

Keywords: Acylation; 2-Methoxynaphthalene; Acetic anhydride; Zeolites; Beta; Polymorph C of Beta; ITQ-17

1. Introduction

Friedel–Crafts acylation processes have been frequently revisited in the last decade since the classical stoichiometric reaction with metal halides [1] is no longer economically and environmentally desired, and the use of alternative recyclable solid acid catalysts is preferred [2–5]. RHODIA has succeeded in a commercial application that involves Y and Beta zeolites for the acylation of anisole and veratrole with acetic anhydride in a fixed-bed continuous reactor [4,5]. Despite the success of zeolites as solid acylation catalysts, they still present limitations in activity when non-activated aromatic compounds must be reacted [6]. Among the different acylation reactions for which zeolites have been applied, the synthesis of *p*-alcoxyacetonaphthones is of special relevance. An example is the synthesis of 2-acetylmethoxynaphthalene (2-AMN), which is intermediate in the synthesis of the anti-inflammatory naproxen (2-(6-methoxy-2-naphthyl)propionic acid, Naproxyn, Syntex) [7].

2-AMN can be manufactured by acylation of 2-methoxynaphthalene (2-MN) with acyl chlorides and $AlCl_3$ as catalyst [7,8]. Acid zeolites have been studied as a potential alternative catalyst, and with these microporous materials the acylation of 2-MN occurs preferentially at the 1-position, producing 1-acetylmethoxynaphthalene (1-AMN) [9], instead of the most desired 2-AMN isomer. It should be possible to increase the selectivity to 2-AMN if one takes into consideration that this isomer has a smaller molecular size than the competing 1-AMN, and can find a zeolite with a pore diameter that allows either a transition state or a diffusion shape selectivity discrimination between the two isomers [9–11]. In this sense, Beta zeolite has shown pore shape effects that are responsible for increasing the selectivity toward the smaller 2-AMN molecule [12]. With Beta zeolite, this isomer is formed preferentially within the pores of Beta while 1-AMN is mainly formed at the external surface. Taking this into account, it is not surprising that the shape selectivity effect is strongly enhanced when the external surface of the Beta crystallites is passivated [13].

Very recently, the pure polymorph C of zeolite Beta has been synthesized either in fluoride or in alkaline media [14], and acidic samples have been produced. This polymorph C has a three-dimensional pore topology with linear 12-MR channels [15]. Two of these channels have a diameter of 0.62×0.66 nm, while the diameter of the third one is 0.63×0.63 nm. This material, named ITQ-17 and with the IZA code BEC [16], presents, a priori, a very interesting pore topology and dimensions for carrying out the acylation of 2-MN. In the present work, we have studied first the diffusivity of the reactant and the two product isomers, i.e., 1-AMN and 2-AMN by molecular dynamics, and the results

* Corresponding author.
E-mail address: acorma@itq.upv.es (A. Corma).

0021-9517/03/$ – see front matter
doi:10.1016/S0021-9517(03)00053-8

have been compared with those obtained with Beta zeolite. Moreover, in other to check the suitability of the theoretical calculations, we have also performed an experimental study of the acylation of 2-MN with acetic anhydride (AA) both in a batch and in a fixed-bed continuous reactors.

2. Experimental

2.1. Materials

Three different ITQ-17 samples BEC-1 to BEC-3 have been synthesized according to [14b], characterized, and studied for the named reaction. A Beta zeolite sample was also synthesized by a seeding process, using nanocrystalline Beta zeolite as seed [17].

The chemical composition of the samples was determined by atomic absorption spectrophotometry (Varian spectrAA-10 Plus). Crystallinity was measured by powder X-ray diffraction, using a Phillips PW1710 diffractometer with Cu-K_α radiation, and compared with a highly crystalline standard sample. Acidity of samples was measured by the standard pyridine adsorption–desorption method [18]. Surface area of catalysts was calculated by the BET/BJH method with N_2 adsorption/desorption performed at 77 K in a Micromeritics ASAP 2000 instrument. Crystal size was determined from SEM (JEOL 6300).

The most relevant physicochemical properties of these zeolites are summarized in Table 1.

2.2. Reaction procedure

2.2.1. Batch reactor

Experiments were made in a 25-ml three-necked round-bottom flask at 405 K, connected to a reflux cooler system, under argon atmosphere and with magnetic stirring. All reagents were supplied by Aldrich. The standard procedure was as follows: 0.17 g of catalyst was activated "in situ" before the reaction by heating for 2 h at 573 K in a vacuum. Then, a mixture of 4.0 mmol of 2-methoxynaphthalene, 2.0 mmol of the acid anhydride (2-MN/AA molar ratio = 2; catalyst/AA ratio = 1 g/12 mmol acetic anhydride), and 3 ml of chlorobenzene was added. Small samples were taken periodically during 24 h. Upon recycling the catalyst, it was observed that deactivation occurs during the reaction.

2.2.2. Fixed-bed reactor

Continuous flow experiments were carried out in a fixed-bed reactor under atmospheric pressure. Typically, 0.50 g of catalyst was pelletized to 0.42–0.59 mm, for which control by internal diffusion was found to be negligible. The catalyst was charged into a quartz reactor (160 mm length, 15 mm i.d.), and activated for 2 h at 773 K in air flow (100 ml min^{-1}), previous to setting the reaction temperature (typically 393 K). A solution of 2-MN (5.70 g, 36.0 mmol) and acetic anhydride (1.84 g, 18.0 mmol) in chlorobenzene (30.00 g) was fed into the reactor at 0.08 g min^{-1} with a syringe pump (2-MN/AA molar ratio = 2; W/F = 217 $g_{CAT}\,h\,mol_{AA}^{-1}$). Reaction samples were collected and weighted at different times on stream (TOS) in a cooling system.

2.2.3. Product characterization

Products were analyzed by GC in a Varian 3350 Series instrument equipped with a 30 m capillary cross-linked 5% phenylmethylsilicone column (HP-5) and a FID detector, using nitrobenzene as internal standard. Products were also identified by mass spectrometry in a Varian Saturn II GC-MS model working with a Varian Star 3400 gas chromatograph and using reference samples. Conversion of 2-MN is referred to as the maximum conversion possible, while the selectivity to the different products is indicated according to the acetonaphthone distribution.

During the reaction, coke-like products were formed in the catalyst, and this became dark brown. Catalysts were extracted in a micro-soxhlet with $CHCl_3$ for 24 h. The solvent was evaporated and the remaining organic material was weighted, diluted with chlorobenzene, and analyzed by GC-MS. Among the adsorbed products we found acetic acid, 2-MN, acetonaphthones, and other by-products. These quantities were considered together with the reaction data obtained for the final crude. Carbon was determinated by ther-

Table 1
Physicochemical characteristics of zeolites tested in the present work

Sample	Si/Ge[a]	(Si + Ge)/Al[a]	Area BET ($m^2\,g^{-1}$)	Micropore volume ($cm^3\,g^{-1}$)	Crystal size (μm)[b]	Acidity (μmol py)[c]					
						Brönsted			Lewis		
						423	523	623	423	523	623
BEC-1	1.2	48	468	0.216	0.6–1.5 × 0.2 × 0.2	20	12	4	1	0	0
BEC-2	9.5	48	436	0.194	0.1–0.2	21	15	8	11	9	8
BEC-3	10.2	73	358	0.143	0.5–1 × 0.2 × 0.2 0.1–0.2	8	6	2	10	9	7
BETA	–	50	484	0.192	1.5–2.5 × 0.2 × 0.2 0.3–0.5	23	20	7	10	7	6

[a] As determined by atomic absorption spectrophotometry.
[b] Average size from the SEM images. Samples BEC-2 and BEC-3: main crystallite size on top. Unusual large crystallite sizes below.
[c] Determined from the infrared spectra of adsorbed pyridine after evacuation at 423, 523, and 623 K.

mogravimetry and elemental analysis in order to quantify the nonextractable organic deposit. In order to determine the nature of the inner carbonaceous compounds the extracted zeolite was dissolved in a 48 wt% solution of hydrofluoric acid [19]. Threefold extraction with chloroform was carried out over the final HF solution, and after evaporation of the solvent the organic material was weighted and analyzed by GC-MS. Furthermore, ultraviolet–visible spectroscopy (Varian Cary 5G UV–VIS-NIR spectrophotometer) was also used to study the functional groups present in the coke. Taking into account all the analyzed products it was possible to obtain mass balances $\geqslant 98\%$.

2.3. Molecular dynamics methodology

Periodic atomistic molecular dynamics (MD) calculations have been performed to simulate the diffusion of 2-MN, and the acylated products in positions 1 and 6, and 1-AMN and 2-AMN in the ITQ-17. The unit cell of ITQ-17 contains 192 atoms (64 SiO_2) and in order to have a larger number of atoms for the molecular dynamics simulations, a $3 \times 3 \times 2$ macrocell containing 3456 atoms was used and 13 molecules of adsorbate were located in the void space of the macrocell in order to complete the system.

The system is equilibrated during a period of 25 ps at a temperature of 450 K with the Berendsen algorithm [20]. After this, runs of 400 ps, with a time step of 1 fs, were carried out within NVE microcanonical ensemble at 450 K. The simulations proceed by first assigning initial velocities to all atoms according to a Maxwell–Boltzmann distribution. The Newton equations of motion are solved using a finite time step by means of the standard Verlet algorithm [21].

In the simulations, every atom was allowed to move explicitly. Although this increases substantially the computational expense, the influence of the framework flexibility has been made clear in a number of studies [22–24], especially when the sorbate matches the pore dimensions, as is the case. The MD simulations have been carried out using the general purpose DL_POLY_2.12 parallel code [25], which was installed on a CRAY-T3E computer at the CIEMAT. The simulations were run using 16 processors. During the simulation, history files were saved every 100 steps, and then mean square displacements were calculated as follows [26],

$$\left\langle X^2(t)\right\rangle = 1/(N_{\mathrm{m}}N_{\mathrm{to}}) \sum_{\mathrm{m}} \sum_{\mathrm{to}} \left[X_i(t+t_0) - X_i(t_0)\right]^2, \qquad (1)$$

where N_{m} is the number of diffusing molecules, N_{to} is the number of time origins used in calculating the average, and X_i is the coordinate of the center of mass of molecule i. The diffusion coefficients, D, were calculated according to [26]

$$\left\langle X^2(t)\right\rangle = 6Dt + B, \qquad (2)$$

where t is the simulation time, and B is the thermal factor arising from atomic vibrations. The trajectories followed by the hydrocarbons in their diffusion path through the zeolite structures are visualized by means of the xy and xz projections, which highlight motion in the different 12 MR (member rings) channels present in ITQ-17.

Four types of interatomic potentials are needed to model this system:

$$V_{\mathrm{total}} = V_{\mathrm{zeolite}} + V_{\mathrm{sorbate}} + V_{\mathrm{sorbate\text{-}sorbate}} + V_{\mathrm{zeolite\text{-}sorbate}}. \qquad (3)$$

The potential for the framework, V_{zeolite}, was originally derived by Catlow et al. [27], and is a Born model potential comprising three-body and short-range terms and long-range Coulomb interactions. The potential for the sorbates, V_{sorbate}, was taken from Oie et al. [28] and comprises two-(bond), three-(angle), and four-body (dihedral) interactions together with Coulomb terms. Finally, 12-6 Lennard-Jones potentials, taken from Catlow et al. [27], and Coulomb interactions were used to describe the sorbate–sorbate and framework–sorbate interactions. The charges for the sorbates were taken from a previous work. More details of the potential parameters [29] and the techniques employed can be found in previous studies [30–34].

3. Results and discussion

3.1. Molecular dynamics

Fig. 1 presents the trajectories of 1-AMN, 2-AMN, and 2-MN through the x and y directions. 1-AMN shows less mobility than 2-AMN and 2-MN and a diffusion more constrained around the local energy minimum position. Among 2-AMN and 2-MN, a much larger diffusivity is observed (with respect to 1-AMN) in both x and y channels, and it is found that the diffusivity is larger for 2-MN than for 2-AMN. Similar conclusions regarding the relative molecular mobilities can be reached by inspection of Fig. 2, in which the x and z directions are shown. These results show that in the case of polymorph C (ITQ-17) the three channels are used for diffusion of 2-AMN and 2-MN, and a significantly slower diffusivity is observed for 1-AMN which does not show large diffusion paths in any of the three channels.

The diffusion coefficients obtained from the molecular dynamics calculations are shown in Table 2. For the correct interpretation of the results and a comparison with previous results [35] found in Beta, a view to the channel dimensions is necessary (Table 2). The channels ⟨100⟩ (which stands for a bidimensional system following directions [100] and [010]) and [001] are interconnected in the two structures, which points to a potentially large microporous space of three interconnected channels for diffusion. Nevertheless, the smaller channel, which correspond to [001] in Beta, is not suitable for diffusion of the large naphthalene rings, and as was seen in a previous paper [35], only the system ⟨100⟩ can be used in Beta for diffusion.

3.1.1. Diffusivity of 1-AMN

Regarding the diffusivity of the 1-AMN, it is seen that this is clearly different in ITQ-17 and Beta. This molecule

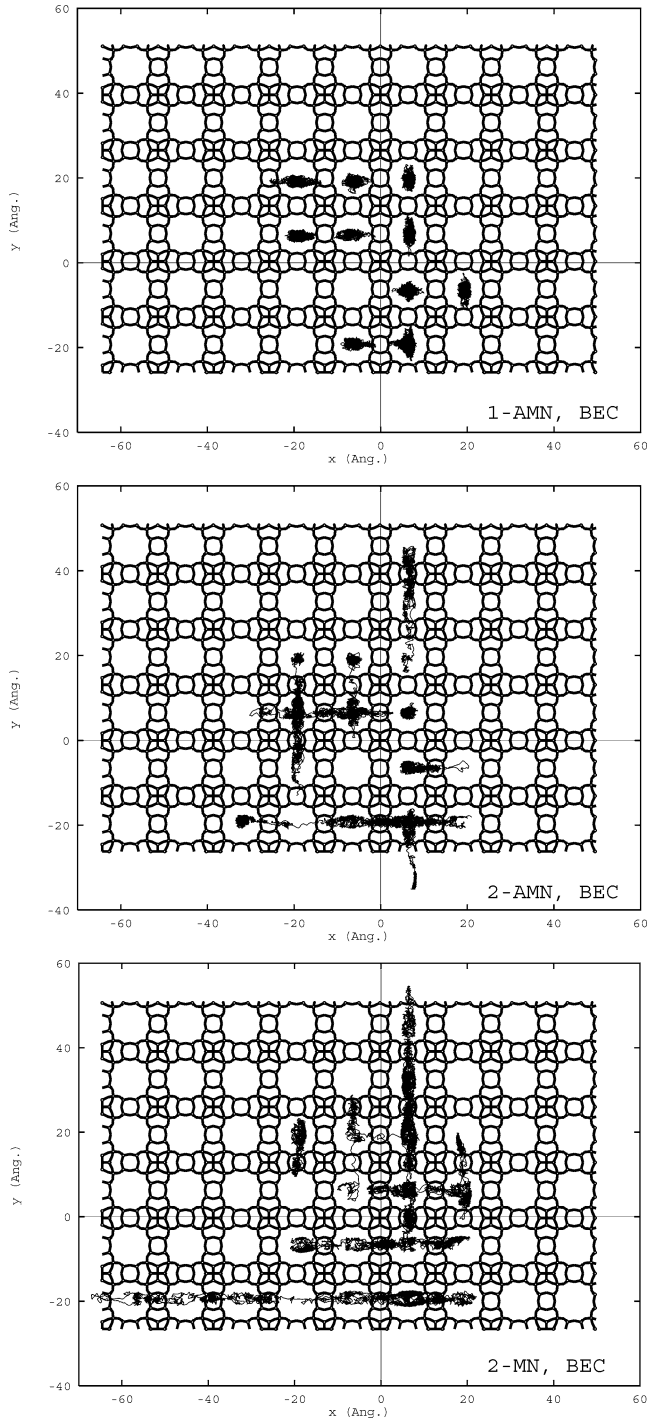

Fig. 1. Trajectories of the center of mass of the 1-AMN, 2-AMN, and 2-MN molecules diffusing through the ITQ-17 structure at 450 K. Projections in xy are shown.

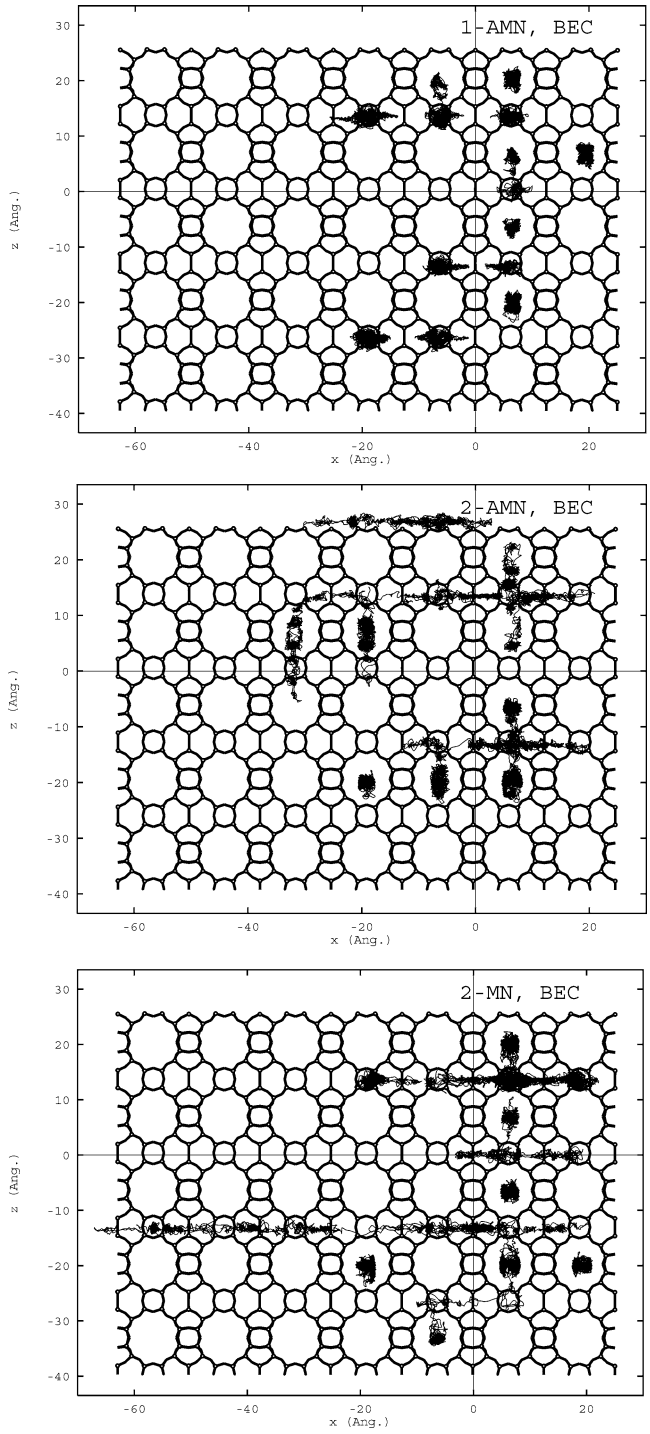

Fig. 2. Trajectories of the center of mass of the 1-AMN, 2-AMN, and 2-MN molecules diffusing through the ITQ-17 structure at 450 K. Projections in xz are shown.

uses mainly the larger channel system ⟨100⟩ and the diffusivity increases substantially in Beta due to the larger size of this system. Although the size is only slightly larger than in ITQ-17, that difference is just about to produce a better fit of 1-AMN in Beta and this justifies the increase in the diffusion coefficients from 0.33 in ITQ-17 to 3.90 in Beta.

3.1.2. Diffusivity of 2-AMN

The size of this molecule is smaller than that of 1-AMN and this results in larger diffusion coefficients. The relative values for the diffusion coefficients of $D_{2\text{-AMN}}$ and $D_{1\text{-AMN}}$ can give information about the selectivity of Beta and BEC polymorphs to these two reaction products, and the results

Table 2
Channel sizes and diffusion coefficients obtained from the molecular dynamics

Structure	Channel size (Å)		Diffusion coefficient (10^{-6} cm^2 s^{-1})		
	⟨100⟩[a]	[001]	2-MN[b] (10.0 × 6.0 × 2.8 Å)	2-AMN (12.3 × 6.2 × 2.8 Å)	1-AMN (10.3 × 8.1 × 4.1 Å)
Beta[c]	6.2 × 7.2	5.5 × 5.5	21.71	10.44	3.90
ITQ-17	6.2 × 6.6	6.3 × 6.3	13.90	9.74	0.33

[a] Two-dimensional channel system running parallel to [100] and [010].
[b] Molecular dimensions in the minimum energy configuration taken from Ref. [12].
[c] Values taken from Ref. [35].

(Table 2) point toward a larger selectivity of the BEC polymorph (ITQ-17) for 2-AMN. As for the diffusional paths, the smaller size of 2-AMN (with respect to 1-AMN) allows the channel [001] in ITQ-17 to be used for diffusion, while this does not occur with the corresponding channel of Beta. Nevertheless, owing to the larger size of the channel system ⟨100⟩ in Beta, this compensates the diffusion restriction in channel [001], up to the point that Beta gives a slightly larger global diffusion coefficient for 2-AMN than ITQ-17.

3.1.3. Diffusivity of 2-MN

The same trends as with 2-AMN are observed and this is due to the fact that although the size of 2-MN is smaller than 2-AMN, both molecules can penetrate the same channel systems (⟨100⟩ in Beta and ITQ-17, and [001] in ITQ-17), and therefore they see the same diffusional space. The smaller size of 2-MN with respect to 2-AMN makes the diffusion coefficients of the former larger.

3.2. Catalytic results

3.2.1. Reaction scheme

The acylation of 2-MN with AA over acid zeolites leads to a complex mixture of products (see [36, Fig. 3]), in which 2-AMN (**I**) is primary stable and 1-AMN (**II**) is primary unstable. At low levels of conversion, and if there are no geometrical constraints, the isomer acylated in 1-position is the most frequent, whereas the other primary product obtained by direct acylation, 2-AMN, is a minority. When increasing conversion, the selectivity to 2-AMN isomers increases due to two secondary reactions: transacylation of 1-AMN with a molecule of 2-MN and protodeacylation of 1-AMN (to produce 2-MN) [37]. At high levels of conversion other reactions also occur. As presented in Fig. 3, **II** can follow an intramolecular transacylation to yield other acetylmethoxynaphthalenes (i.e., 1-acetyl-7-methoxynaphthalene, **III**) [37], while consecutive acylation of the monoacylated products is also possible [19] producing different isomers of the diacetylmethoxynaphthalene (dAMN, **IV**). We have

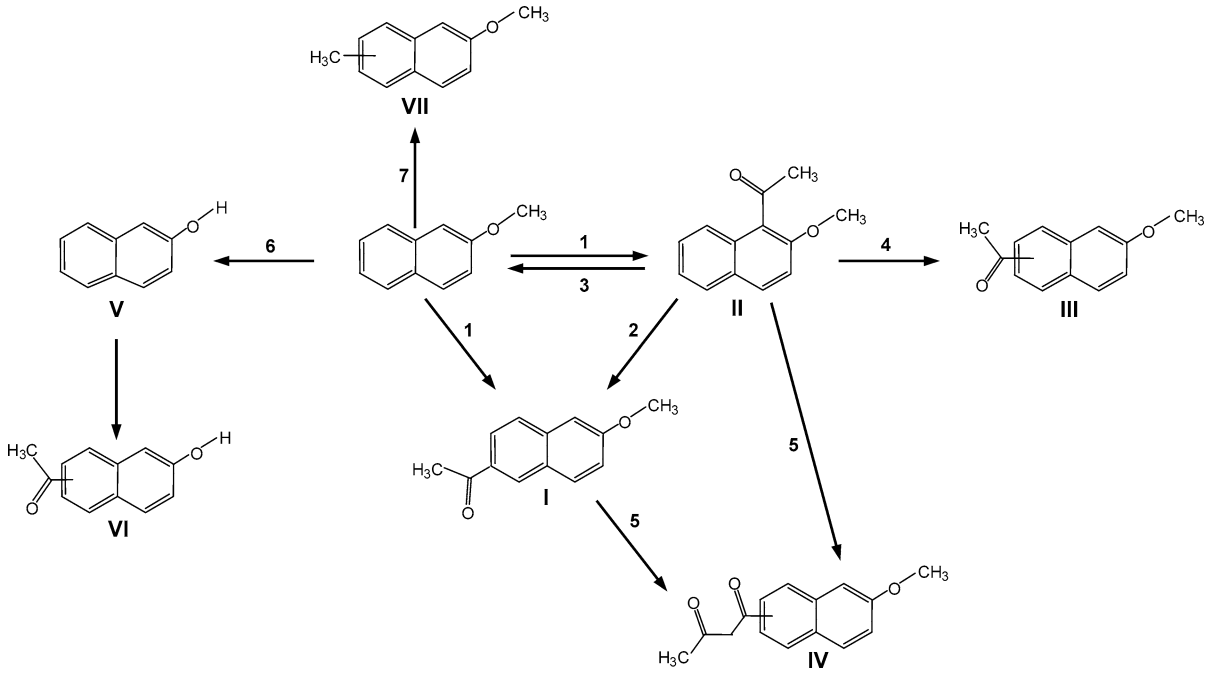

Fig. 3. Reaction scheme of the acylation of 2-MN with acetic anhydride over zeolites and possible alternative processes: (1) direct acylation; (2) intermolecular transacylation of 1-AMN with 2-MN; (3) protodeacylation of 1-AMN; (4) intramolecular transacylation of 1-AMN; (5) consecutive acylation of monoacylated products; (6) hydrolysis of the terminal O–C bond of 2-MN; (7) transalkylation of 2-MN.

Table 3
Acylation of 2-methoxynaphthalene with acetic anhydride over ITQ-17 (main families of the most frequent products detected by GC-MS)

Family	Chemical structure	Assignation	FW[a]	Products
Primary acetylmethoxynaphthalenes	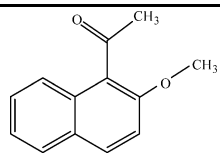	1-AMN	200	1
	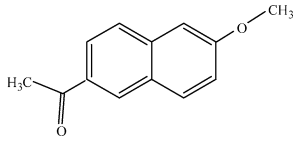	2-AMN	200	1
Secondary acetylmethoxynaphthalenes	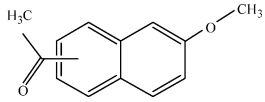	AMN	200	3
Diacylmethoxynaphthalenes	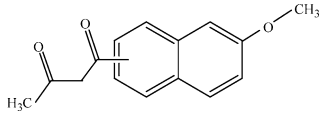	dAMN	242	2
2-Naphthol and acylderivatives	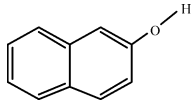	2-NOH	144	1
	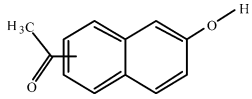	2-ANOH	186	2
Methylmethoxynaphthalene	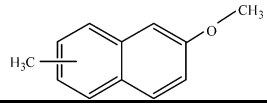	MMN	172	1

[a] Formular weight obtained by mass spectrometry.

to point out that in a few experiments, products coming from the hydrolysis of the 2-MN in the crude, 2-naphthol (2-NOH, **V**) and two different acylated derivatives (acetylnaphthols, 2-ANOH, **VI**), have been detected. The hydrolysis of the terminal O–C bond in aryl ethers has been described over zeolites containing important amounts of extraframework aluminum (EFAL). The presence of traces of water remaining in the catalyst even after the activation step produces the hydrolysis of strong Lewis acid sites (electron-deficient centers) releasing strong Brönsted acid sites [38, 39]. These last ones are able to catalyze the demethylation of 2-MN to 2-NOH. Such a demethylation process generates methyl groups in the reactant medium, which can either be released as methanol or intervene in a transalkylation mechanism leading to methyl derivatives of 2-MN. In fact, one methyl isomer of 2-MN (**VII**) was found occasionally in the crude. According to all these processes, a list of the different families of products identified by the GC-MS and their characteristics is given in Table 3. All products were taken into account for the calculation of the conversion and selectivity.

3.2.2. Comparison of the catalytic behavior of polymorphs A plus B (Beta) and polymorph C (ITQ-17)

The molecular dynamics study predicts a lower diffusivity of 2-MN in ITQ-17 than in Beta, and this may result in a lower activity of the former if the diffusion of reactants within the pores is slower than the reaction. To check this, the initial acylation rate of 2-MN (rate of formation of 1-AMN plus 2-AMN) was measured with BEC-1 and Beta samples, both with similar crystal sizes and T^{IV}/T^{III} ratios (see Table 1). The results obtained (Table 4 and Fig. 4) show that indeed ITQ-17 is less active than Beta. On the other hand, the ratios of the diffusion coefficients of 2-AMN and 1-AMN calculated preclude that shape selectivity for the diffusion of products should exist. Indeed, the slower diffusion of 1-AMN will allow this product to suffer secondary reactions in a larger extent than 2-AMN and, following the reaction scheme presented before, this should result in an increased selectivity toward 2-AMN. From the theoretical calculations, the shape selectivity effect for product diffusion should be larger in ITQ-17 than in Beta, and this should

Table 4
Acylation of 2-methoxynaphthalene with acetic anhydride over ITQ-17 in a batch reactor and comparison with Beta zeolite[a]

Catalyst	$r_{1\text{-AMN}}$[b]	$r_{2\text{-AMN}}$[b]	r_{AMN}[b]	$S_{1\text{-AMN}}$[c] (M%)	$S_{2\text{-AMN}}$[c] (M%)	S_{AMN}[c] (M%)	X_{T} 2-MN 24 h (M%)[d]	$S_{1\text{-AMN}}$[d] (M%)	$S_{2\text{-AMN}}$[d] (M%)	S_{AMN}[d] (M%)	$S_{2\text{-NOH}}$[d] (M%)	$S_{2\text{-dAMN}}$[d] (M%)
BEC-1	15.38	19.39	0	44.2	55.8	0	28	35.7	62.9	1.4	0	0
BEC-2	26.37	21.28	0	55.3	44.7	0	67	44.7	49.8	4.8	0	0.7
BEC-3	38.44	16.14	0	70.4	29.6	0	52	61.4	34.5	3.5	0	0.5
BETA	54.46	41.74	4.24	54.2	41.6	4.2	90	32.1	54.7	11.5	0.4	1.3

[a] Experimental data: solvent, chlorobenzene; $T = 405$ K; catalyst/$Ac_2O = 1$ g/12 mmol; 2-MN/AA = 2/1 (M).
[b] Initial reaction rate in mmol g^{-1} h^{-1} at ∼15% conversion.
[c] From the initial reaction rates.
[d] 2-MN conversion and corresponding selectivities to the different products in the final crude.

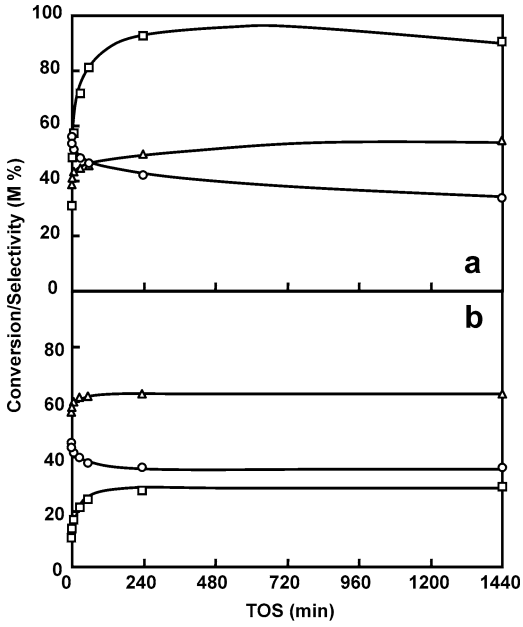

Fig. 4. Acylation of 2-MN with AA in a batch reactor over Beta (a) and BEC-1 (b) samples (see Table 1). Conversion of 2-MN (□) and selectivities to 2-AMN (△) and 1-AMN (○). Experimental conditions: solvent, chlorobenzene; $T = 405$ K; catalyst/$Ac_2O = 1$ g/12 mmol; 2-MN/AA = 2:1 (M).

result in a higher ratio of 2-AMN/1-AMN in the products obtained with the former. The results from Table 4 agree with the hypothesis even when considering the results after 24 h reaction time.

While the results look consistent in a first approximation, there is one factor that has not been considered when comparing the catalytic results with the two samples. This is the fact that BEC-1 contains Ge^{IV}, while Beta zeolite does not. The presence of framework Ge will decrease the average Sanderson electronegativity of the zeolite [40] with the corresponding decrease in the acid strength of the Brönsted acid sites. Moreover, large amounts of Ge in the framework can decrease the stability of the zeolite resulting in a larger loss of crystallinity upon activation. Taking into account the micropore volume of BEC-1 and Beta samples (Table 1) we believe that BEC-1 still preserves its integrity after activation. On the other hand, the acidity as measured by the pyridine adsorption–desorption method shows that the number of Brönsted acid sites retaining pyridine at the lowest temperature (423 K), which are of weak, medium and strong acidity [41], are proportionally closer in the two zeolites than the stronger ones retaining pyridine at 523 K and even more so at 623 K. This would be in agreement with the presence of Ge that produces a decrease in the acid strength of the zeolite. Since acid sites with weak and medium strength can already catalyze this reaction [42], we could assume that differences in activity and selectivity observed are not due to differences in acid strength but differences in reactant and product diffusivities in the two zeolites.

In order to support or reject this, a ITQ-17 sample with the same T^{IV}/T^{III} ratio, but with smaller average crystal size (as measured by SEM, Fig. 5), was prepared (BEC-2). This sample, contrary to BEC-1, possesses a bimodal crystal size, with $>$ 80% of the crystals with a diameter of 0.1–0.2 μm, and the $<$ 20% left with crystal size of $0.5–1 \times 0.2 \times 0.2$ μm. Globally the crystal size of the BEC-2 is smaller than that of the BEC-1, which shows a more uniform size distribution of $0.6–1.5 \times 0.2 \times 0.2$ μm. BEC-2 has a higher Si/Ge ratio than BEC-1 (Table 1) and it presents some higher acid strength than BEC-1, and in the range of Beta. The catalytic results obtained with BEC-2 show that it still presents a relatively higher initial selectivity to 2-AMN than Beta, but lower than BEC-1. Meanwhile, the initial reaction rate for BEC-2 is higher than for BEC-1 but still lower than Beta. These catalytic results can be easily explained by assuming that this reaction is controlled by diffusion at the zeolite pores and, therefore, the smaller crystallite size of BEC-2, that implies a larger ratio of external to internal surface, should give an increase in activity and a decrease in the selectivity to 2-AMN.

The important effect of crystal size in a process like this, which is controlled by the diffusion of reactants and products within the pores of the zeolites, could be corroborated with a new sample (BEC-3) with practically the same Si/Ge ratio than BEC-2 but with a higher T^{IV}/T^{III} ratio (and consequently with lower acidity, see Table 1) and a smaller crystallite size. The initial reaction rate (Table 4) shows that even if the number of acid sites is much lower in BEC-3 than in the other BEC samples, its catalytic activity is still large. This result can only be explained considering the beneficial role of the higher ratio of external to internal surface

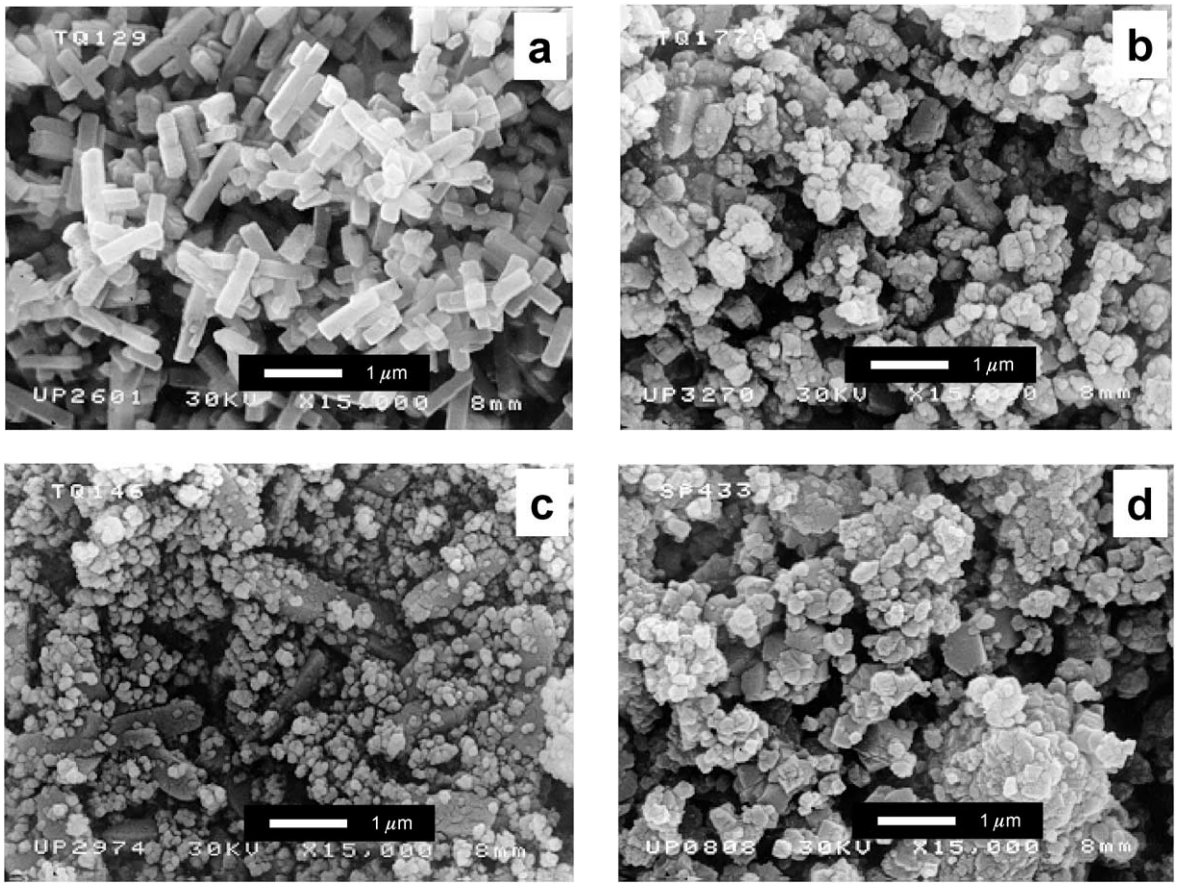

Fig. 5. SEM micrographs of zeolites tested in the present work. (a) BEC-1; (b) BEC-2; (c) BEC-3; (d) Beta.

on catalyst activity. At the same time, this variable has a negative effect on the selectivity to 2-AMN. After all, from the catalytic results obtained when working in a batch reactor, we can conclude that, in agreement with the molecular dynamics study, the pore dimensions and topology of the polymorph C of Beta (ITQ-17) should present a larger diffusion resistance for the reactant (2-MN) than the polymorphs A and B of Beta (despite the fact that 2-MN does not diffuse in one of the channels of Beta with dimensions 5.5×5.5 Å), which corresponds with the lower activity observed and the strong effect of crystallite size on conversion. Also, the larger relative diffusion coefficient for 2-AMN and 1-AMN in polymorph C than in polymorphs A and B would explain the higher selectivity to the former product in ITQ-17 samples with larger crystallites and the lower when the crystallite size decreases and the external surface, which is the main responsible for formation of 1-AMN, starts to play a predominant role.

Nevertheless, it is well known that when working in a batch reaction it becomes difficult to uncouple catalyst activity from catalyst decay. Thus, in a case like this, where the blocking of pores may readily occur, catalyst decay can have an important impact on conversion and selectivity. From these considerations, we decided to perform the reaction also in a continuous fixed-bed reactor system, and the results will be presented below.

3.2.3. Acylation of 2-MN with AA in a continuous fixed-bed reactor

2-MN has been acylated with AA by working in liquid phase at 393 K in a continuous fixed-bed reactor, using BEC-2 and Beta as catalysts. The results presented in Fig. 6a show that a decay of the catalyst with the time of stream (TOS) occurs in the two samples. However, it is remarkable that at short TOS the activity of the two catalysts is similar. This is different from that observed when working in the batch reactor and will point to the fact that catalyst decay is faster for BEC-2 than for Beta, probably due to the narrower pores in the former, and also to a faster deactivation of the sites at the external surface. With respect to selectivity, the ratio 2-AMN/1-AMN (Figs. 6b and 6c) clearly shows a higher selectivity to the desired product with ITQ-17. Moreover, the ratio slightly increases with TOS, indicating that the rate of deactivation is proportionally larger at the crystallite surface, where the 1-AMN is preferentially formed.

The total amount of organic products remaining adsorbed on the deactivated catalyst after soxhlet extraction with chloroform was determined by thermogravimetry as well as by elemental analysis, and the results are given in Tables 5 and 6. It can be seen there that for similar levels of conversion the amount of organic products remaining adsorbed is higher in ITQ-17 than in Beta zeolite, which can be consistent with a faster blocking of surface and pores, and

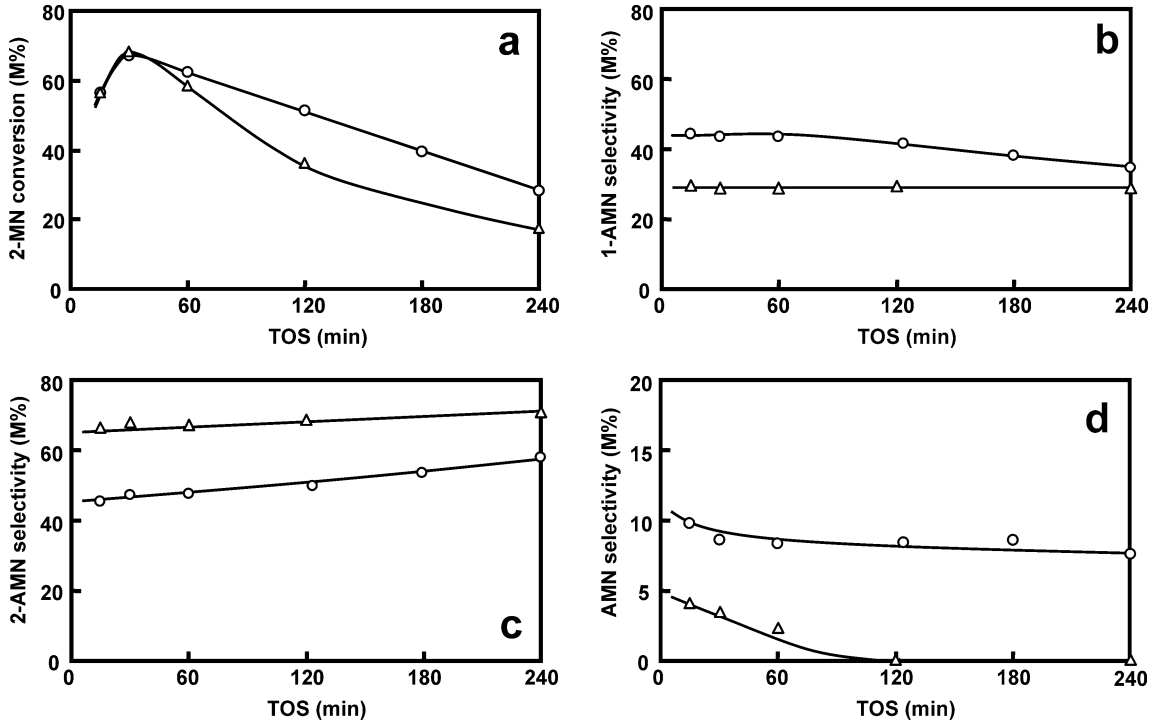

Fig. 6. Acylation of 2-MN with AA in a fixed-bed reactor over Beta (○) and BEC-2 (△) samples (see Table 1). (a) Conversion of 2-MN; (b) selectivity to 1-AMN; (c) selectivity to 2-AMN; (d) selectivity to other AMN. Experimental conditions: solvent, chlorobenzene; $T = 393$ K; $W/F = 217\ g_{CAT}\,h\,mol_{AA}^{-1}$; 2-MN/AA = 2/1 (M).

Table 5
Amount and composition of the organic deposit found in ITQ-17 and Beta samples after 2-MN/AA acylation in a batch reactor[a]

Catalyst	Soxhlet extract						Liquid phase[b]					Residue after extraction[c]						
	wt%	1-AMN (M%)	2-AMN (M%)	AMN (M%)	2-NOH (M%)	dAMN (M%)	1-AMN (M%)	2-AMN (M%)	AMN (M%)	2-NOH (M%)	dAMN (M%)	TG (wt%)	AE (C%)	1-AMN (M%)	2-AMN (M%)	AMN (M%)	2-NOH (M%)	dAMN (M%)
BEC-1	1.1	0	100	0	0	0	35.6	63.0	1.4	0	0	3.7	3.1	nd[d]	nd	nd	nd	nd
BEC-2	1.9	26	71	3	0	0	44.3	50.3	4.7	0	0.7	6.9	7.4	0	94	0	0	6
BETA	1.1	15	60	7	3	4	32.0	54.8	11.4	0.4	1.4	5.6	5.2	0	61	0	0	39

[a] Reaction conditions: solvent, chlorobenzene; $T = 405$ K; catalyst/AA = 1 g/12 mmol; 2-MN/AA = 2/1 (M).
[b] Product distribution determined by considering the quantity of every product obtained in the reaction crude plus those products obtained by soxhlet extraction.
[c] Product distribution obtained after HF treatment of the extracted zeolite. Data are only semiquantitative.
[d] Not determined.

Table 6
Amount and composition of the organic deposit found in ITQ-17 and Beta samples after 2-MN/AA acylation in a fixed-bed reactor[a]

Catalyst	Soxhlet extract						Residue after extraction[b]						
	wt%	1-AMN (M%)	2-AMN (M%)	AMN (M%)	2-NOH (M%)	dAMN (M%)	TG (wt%)	AE (C%)	1-AMN (M%)	2-AMN (M%)	AMN (M%)	2-NOH (M%)	dAMN (M%)
BEC-2	7.0	11	69	5	0	15	3.8	4.5	0	81	0	0	19
BETA	13.7	20	64	8	2	6	3.5	3.4	0	31	0	0	69

[a] Reaction conditions: solvent, chlorobenzene; $T = 405$ K; catalyst/AA = 1 g/12 mmol; 2-MN/AA = 2/1 (M).
[b] Product distribution obtained after HF treatment of the extracted zeolite. Data are only semiquantitative.

consequently with a faster catalytic decay in ITQ-17. The nature of the adsorbed products has been determined after destroying the zeolitic part by a HF treatment [19]. The results (Tables 5 and 6) show that regardless of the reactor system used, the organic deposit in ITQ-17 is always richer in 2-AMN than in Beta.

3.2.4. Influence of reaction temperature in the fixed-bed continuous operation on 2-AMN selectivity

An increase in the reaction temperature is expected to enhance the selectivity to 2-AMN, as the isomerization of 1-AMN into 2-AMN and the protodeacylation of 1-AMN will be favored [37]. For this reason, one experiment was

Table 7
Acylation of 2-methoxynaphthalene with acetic anhydride in a fixed-bed reactor over BEC-2 samples at different reaction temperatures[a]

Temperature (K)	X_T 2-MN (M%)	$S_{1\text{-AMN}}$ (M%)	$S_{2\text{-AMN}}$ (M%)	S_{AMN} (M%)	$S_{2\text{-NOH}}$ (M%)	$S_{2\text{-dAMN}}$ (M%)	X_T max 2-MN (M%)[c]	$S_{1\text{-AMN}}{}^c$ (M%)	$S_{2\text{-AMN}}{}^c$ (M%)	$S_{AMN}{}^c$ (M%)	$S_{2\text{-NOH}}{}^c$ (M%)	$S_{2\text{-dAMN}}{}^c$ (M%)
393	17.2	34.0	66.0	0	0	0	68.3	28.8	67.8	3.4	0	0
493	17.0	5.3[b]	13.7[b]	0[b]	81.0[b]	0[b]	50.3	0	0	0	100	0

[a] Reaction conditions: solvent, chlorobenzene; $W/F = 217\ g_{CAT}\,h\,mol^{-1}_{AA}$; 2-MN/AA = 2/1 (M).

[b] Interpolated data.

[c] Maximum conversion of 2-MN reached and selectivities corresponding to the different products.

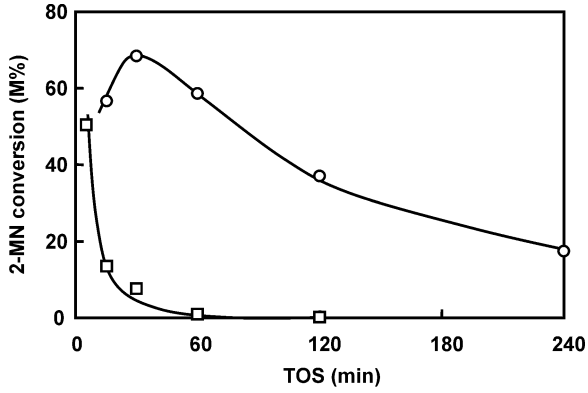

Fig. 7. Conversion of 2-MN at $T = 393$ K (○) and 493 K (□) in the acylation of 2-MN with AA in a fixed-bed reactor over BEC-2 sample. Other experimental conditions: solvent, chlorobenzene; $W/F = 217\ g_{CAT}\,h\,mol^{-1}_{AA}$; 2-MN/AA = 2/1 (M).

carried out at 493 K, in gas phase, and the catalytic results are comparatively shown in Fig. 7 and Table 7. The increase of temperature gives undesirable reaction products coming from the hydrolysis of the methoxy group of the 2-MN ring, that produces 2-NOH and 2-ANOH. Although the relative selectivity of 2-AMN to 1-AMN increases slightly (2-AMN/1-AMN ratio of 2.6 at 493 K, 2.3 at 393 K), the global evolution of the process when increasing the temperature is negative owing to the production of demethylated products (Table 7) and to a faster decay of the catalyst. This decay is parallel to a larger deposition of organic residues on the catalyst when working at higher temperatures.

The reaction temperature also determines the nature of the organic residue in the used catalyst. Thus, most of the carbonaceous compounds adsorbed at 393 K can be easily extracted in a micro-soxhlet with chloroform, whereas the sample reacted at 493 K shows a much larger amount of irreversibly adsorbed products (coke) (12.6 wt% vs 3.8 wt% in the catalyst tested at 393 K, as determined by thermogravimetry). This coke is of a more condensed in nature, and must be mainly constituted by polyacylated and polyaromatic compounds [6], which cannot be detected by GC-MS, even after destroying the zeolite with HF.

4. Conclusions

The diffusion coefficients obtained from molecular dynamics calculations show different diffusivities for reactant (2-MN) and products (1-AMN and 2-AMN) in the pores of the polymorphs A and B of Beta and in the polymorph C (ITQ-17). The larger diameter of the channel system ⟨100⟩ in polymorphs A and B with respect to C produces a increase in the diffusivity of the reactant 2-MN.

The ratio of the diffusion coefficients for 2-AMN to 1-AMN is one order of magnitude larger within polymorph C than with polymorphs A and B, precluding a larger shape selectivity effect in the selectivity to 2-AMN.

Catalytic results in batch and fixed bed continuous reactor show that the polymorph C (ITQ-17) is less active than Beta due to the lower diffusivity of the reactant in the pores of ITQ-17 and to a faster catalytic decay. Meanwhile, and in agreement with the theoretical results, the selectivity to 2-AMN is larger in ITQ-17.

The analysis of the organic products remaining adsorbed within the zeolites pores after the reaction shows that 2-AMN remains occluded after soxhlet extraction and the total amount is larger in ITQ-17 than in Beta zeolite.

Only a marginal increase in selectivity to 2-AMN was observed when increasing the reaction temperature. The reaction is then carried out in gas phase and the contribution of the undesirable reactions to the process as well as the deposition of organic residues in the catalyst increases strongly, leading to a faster decay.

Acknowledgments

The authors thank the Comisión Interministerial de Ciencia y Tecnología (CICYT) in Spain (Project MAT2000-1392) for financial support and the CIEMAT (Centro de Investigaciones Energeticas, Medio Ambientales y Tecnológicas) for the use of its computing facilities.

References

[1] G.A. Olah, Friedel–Crafts and Related Reactions, Vols. I–IV, Wiley, New York, 1963–1964.
[2] A. Corma, Chem. Rev. 95 (1995) 559.
[3] P.B. Venuto, Micropor. Mater. 2 (1994) 297.
[4] M. Spagnol, L. Gilbert, D. Alby, Ind. Chem. Libr. 8 (1996) 29.
[5] (a) M. Spagnol, L. Gilbert, E. Benazzi, C. Marcilly, Patent PCT, Int. Appl. WO 97 35656 A1, 1996;
(b) M. Spagnol, L. Gilbert, E. Benazzi, C. Marcilly, Patent PCT, Int. Appl. WO 96 35655 A1, 1996.

[6] P. Botella, A. Corma, J.M. López-Nieto, J. Catal. 195 (2000) 161.
[7] C. Giordano, European patent Appl. EP 301311, 1989.
[8] C. Kuroda, Sci. Papers Phys. Chem. Res. 18 (1932) 51.
[9] (a) G. Harvey, G. Mader, Collect. Czech. Chem. Commun. 57 (1992) 862;
(b) G. Harvey, G. Binder, R. Prins, Stud. Surf. Sci. Catal. 94 (1995) 397.
[10] H.K. Heinichen, W.F. Hölderich, J. Catal. 185 (1999) 408.
[11] M. Neuber, E.I. Leupold, European patent Appl. EP 459495 B1, 1991.
[12] P. Bharathi, S.B. Waghmode, S. Sivasanker, R. Vetrivel, Bull. Chem. Soc. Jpn. 72 (1999) 2161.
[13] P. Andy, J. García-Martínez, G. Lee, H. González, C.W. Jones, M.E. Davis, J. Catal. 192 (2000) 215.
[14] (a) A. Corma, M.T. Navarro, F. Rey, J. Rius, S. Valencia, Angew. Chem. Int. Ed. 40 (2001) 2277;
(b) A. Corma, M.T. Navarro, F. Rey, S. Valencia, Chem. Commun. (2001) 1486.
[15] T. Conradsson, M.S. Dadachov, X.D. Zou, Micropor. Mesopor. Mater. 41 (2000) 183.
[16] W.M. Meier, D.H. Olson, Ch. Baerlocher, Atlas of Zeolite Structure Types, 4th ed., Elsevier, Amsterdam, 1996. Also in the web, http://www.iza-sc.ethz.ch/IZASC/Atlas/AtlasHome.html.
[17] P. Botella, A. Corma, J.M. López-Nieto, S. Valencia, M.E. Lucas, M. Sergio, Appl. Catal. A: Gen. 203 (2000) 251.
[18] A. Chica, A. Corma, J. Catal. 187 (1999) 167.
[19] D. Rohan, C. Canaff, E. Fromentin, M. Guisnet, J. Catal. 177 (1998) 296.
[20] H.J.C. Berendsen, J.P.M. Postma, W. van Gunsteren, A. DiNola, J.R. Haak, J. Chem. Phys. 81 (1984) 3684.
[21] L. Verlet, Phys. Rev. 159 (1967) 98.
[22] P. Demontis, E.S. Fois, G.B. Suffriti, S.J. Quartieri, Phys. Chem. 94 (1990) 4329.
[23] M.W. Deem, J.M. Newsam, J.A. Creighton, J. Am. Chem. Soc. 114 (1992) 7198.
[24] G. Sastre, C.R.A. Catlow, A. Corma, J. Phys. Chem. B 103 (1999) 5187.
[25] W. Smith, T.R. Forester, J. Mol. Graph. 14 (1996) 136.
[26] M.P. Allen, D. Tildesley, Molecular Simulation of Liquids, Oxford Univ. Press, Oxford, 1980.
[27] C.R.A. Catlow, C.M. Freeman, B. Vessal, S.M. Tomlinson, M. Leslie, J. Chem. Soc., Faraday Trans. 87 (1991) 1947.
[28] T. Oie, T.M. Maggiora, R.E. Christoffersen, D.J. Duchamp, Int. J. Quantum Chem., Quantum Biol. Symp. 8 (1981) 1.
[29] G. Sastre, N. Raj, C.R.A. Catlow, R. Roque-Malherbe, A. Corma, J. Phys. Chem. B 102 (1998) 3198.
[30] S. Yashonat, J.M. Thomas, A.K. Nowak, A.K. Cheetham, Nature 331 (1988) 601.
[31] G. Schrimpf, M. Schlenkrich, J. Brickmann, P. Bopp, J. Phys. Chem. 96 (1992) 7404.
[32] J.B. Nicholas, F.R. Trouw, J.E. Mertz, L.E. Iton, A.J. Hopfinger, J. Phys. Chem. 97 (1993) 4149.
[33] S.M. Auerbach, N.J. Henson, A.K. Cheetham, H.I. Metiu, J. Phys. Chem. 99 (1995) 10600.
[34] G. Sastre, C.R.A. Catlow, A. Chica, A. Corma, J. Phys. Chem. B 104 (2000) 416.
[35] P. Botella, A. Corma, G. Sastre, J. Catal. 197 (2001) 81.
[36] H.W. Kouwenhoven, H. van Bekkum, in: G. Ertl, H. Knözinger, J. Weitkamp (Eds.), Handbook of Heterogeneous Catalysis, Vol. 5, VCH, Weinheim, 1997, p. 2358.
[37] (a) E. Fromentin, J.-M. Coustard, M. Guisnet, J. Catal. 190 (2000) 433;
(b) V. Moreau, E. Fromentin, P. Magnoux, M. Guisnet, Stud. Surf. Sci. Catal. 135 (2001) 4113.
[38] C. Flego, G. Pazzuconi, C. Perego, Stud. Surf. Sci. Catal. 142B (2002) 1603.
[39] P. Botella, A. Corma, F. Rey, S. Valencia, Stud. Surf. Sci. Catal. 142A (2002) 651.
[40] W.J. Mortier, J. Catal. 55 (1978) 138.
[41] G. Bourdillon, C. Gueguen, M. Guisnet, Appl. Catal. 61 (1990) 123.
[42] E.A. Gunnewegh, S.S. Gopie, H. van Bekkum, J. Mol. Catal. A: Chem. 106 (1996) 151.